PAPER

Quantum oscillations with angular dependence in PdTe$_2$ single crystals

View the article online for updates and enhancements.

Quantum oscillations with angular dependence in PdTe₂ single crystals

Ramakanta Chapai[1] , **D A Browne**[1], **David E Graf**[2], **J F DiTusa**[1] **and Rongying Jin**[1,*]

[1] Department of Physics and Astronomy, Louisiana State University, Baton Rouge, LA 70803, United States of America
[2] National High Magnetic Field Laboratory, Tallahassee, FL 32310, United States of America

E-mail: rjin@lsu.edu

CrossMark

Abstract

The layered transition-metal dichalcogenide PdTe₂ has been discovered to possess bulk Dirac points as well as topological surface states. By measuring the magnetization (up to 7 T) and magnetic torque (up to 35 T) in single crystalline PdTe₂, we observe distinct de Haas–van Alphen (dHvA) oscillations. Eight frequencies are identified with $H||c$, with two low frequencies ($F_\alpha = 8$ T and $F_\beta = 117$ T) dominating the spectrum. The effective masses obtained by fitting the Lifshitz–Kosevich (LK) equation to the data are $m^*_\alpha = 0.059m_0$ and $m^*_\beta = 0.067m_0$ where m_0 is the free electron mass. The corresponding Landau fan diagrams allow the determination of the Berry phase for these oscillations resulting in values of $\sim 0.67\pi$ for the 3D α band (hole-type) (down to the 1st Landau level) and $\sim 0.23\pi$–0.73π for the 3D β band (electron-type) (down to the 3rd Landau level). By investigating the angular dependence of the dHvA oscillations, we find that the frequencies and the corresponding Berry phase (Φ_B) vary with the field direction, with a $\Phi_B \sim 0$ when H is 10°–30° away from the ab plane for both α and β bands. The multiple band nature of PdTe₂ is further confirmed from Hall effect measurements.

Keywords: topological materials, de Haas–van Alphen oscillations, Landau levels, Berry phase

S Supplementary material for this article is available online

(Some figures may appear in colour only in the online journal)

1. Introduction

Due to the versatility of crystal symmetry operations, condensed matter systems are fertile ground to realize new physics involving novel particle excitations such as Dirac fermions [1–3], Weyl fermions [4, 5], Majorana fermions [6, 7], and even more complex or exotic fermions [8, 9]. Realizing these excitations in solids not only offers opportunities to investigate the fundamental physics associated with these excitations, but also provides powerful routes towards potential applications such as quantum computing and spintronic technolo-

gies [10–12]. In this regard, materials with unique quantum mechanical properties such as topological insulation and topological superconductivity have attracted a great deal of recent attention [13, 14]. Among quantum materials, the layered transition metal dichalcogenides (TMDs) present a wide variety of intriguing properties. For example, the coexistence of type-I Dirac fermions and type-II Dirac fermions has been reported in some layered TMDs [15]. In type-I Dirac fermion systems, the valence and conduction bands meet at the Dirac point and Lorentz invariance is obeyed. In contrast, type-II Dirac fermions break Lorentz invariance because of the tilting of the Dirac cones [16]. Consequently, new quantum phenomena such as the angle dependent chiral anomaly and topological

* Author to whom any correspondence should be addressed.

1

Table 1. A list of frequency F (in the unit of tesla) and Berry phase Φ_B (in the unit of π) that have been detected from de Haas–van Alphen (dHvA) and Shubnikov–de Haas (SdH) oscillations in PdTe$_2$ with $H||c$.

| This work (dHvA) | | Reference [21] (dHvA) | | Reference [24] | | | Reference [25] (dHvA) | Reference [26] (dHvA) | | Reference [27] (dHvA) | Reference [28] (dHvA) |
| | | | | dHvA | | SdH | | | | | |
F	Φ_B	F	Φ_B	F	Φ_B	F	F	F	Φ_B	F	F
8 (α)	0.67	8.0	0.92	8	1.14	—	—	9.13	0.72	9	—
—	—	—	—	109	—	—	—	—	—	—	—
—	—	113.2	—	113	—	—	—	112.7	—	112	—
117 (β)	0.23	117.9	—	117	—	—	121.5	—	—	—	—
—	—	124.3	—	127	—	—	—	—	—	—	125
133 (γ)	—	133.9	—	133	—	—	—	—	—	—	—
141 ($\alpha + \gamma$)	—	—	—	140	—	—	—	—	—	—	—
242 ($\alpha + 2\beta$)	—	—	—	—	—	—	239	228.7	—	—	—
272 (η)	—	—	—	—	—	—	283.2	—	—	—	—
360 (ζ)	—	—	—	—	—	—	—	—	—	—	—
462 ($\wp$)	—	455.8	—	455	—	—	—	456.9	—	459	460
—	—	—	—	—	—	920	—	913.9	—	—	—
2468 (ϑ)	—	—	—	—	—	2350	—	—	—	—	2260
2588 (ξ)	—	—	—	—	—	2675	—	2568	—	2577	2560

phase transitions are expected in the type-II Dirac fermion systems [16–20].

The presence of type-II Dirac fermions in PdTe$_2$ was recently predicted by first principles calculations and observed in angle-resolved photoemission spectroscopy (ARPES) [17, 21]. In addition to possessing topologically non-trivial bulk bands and topological surface states [15, 22], PdTe$_2$ exhibits superconductivity as well (with $T_c \sim 1.7$ K [21, 23]). Thus, it is likely a candidate for topological superconductivity [21]. However, there is considerable disparity in experimental results in literature. As summarized in table 1, we note that (1) some frequencies obtained from quantum oscillations are not consistent with each other [21, 24–28], (2) there is large discrepancy in the Berry phase for the smallest band [21, 24–26], and (3) there is little information about the larger bands other than the one with the lowest frequency. These conflicting results call for continued examination of the physical properties of PdTe$_2$. This is in part due to its complex Fermi surface and the associated difficulty in identifying the contribution of each Fermi surface pocket to the overall transport properties [21, 24, 25]. It has also not been addressed whether these discrepancies are related to sample quality (composition and crystallinity). Moreover, a measurement of the angle dependence of the Berry phase, which is crucial to understand the Fermi surface topology, has not been reported.

Here, we describe the results of an experimental investigation of the magnetotransport (magnetoresistance and Hall effect) and magnetic (magnetization and magnetic torque) properties of PdTe$_2$ to explore the nature of the electronic excitations. By analyzing the de Haas–van Alphen (dHvA) oscillations found in both the magnetization and magnetic torque at low temperatures, eight frequencies are identified: $F_\alpha = 8$ T, $F_\beta = 117$ T, $F_\gamma = 133$ T, $F_\eta = 272$ T, $F_\zeta = 360$ T, $F_\wp = 462$ T, $F_\vartheta = 2468$ T, and $F_\xi = 2588$ T. The presence of multiple Fermi surface pockets is further confirmed by the

Hall resistivity, which varies nonlinearly with the applied magnetic field. Using the Lifshitz–Kosevich (LK) equation [29] to fit experimental data, the effective masses of the respective bands are found as: $m_\alpha^* = 0.059m_0$, $m_\beta^* = 0.067m_0$, $m_\gamma^* = 0.084m_0$, $m_\eta^* = 0.107m_0$, and $m_\zeta^* = 0.120m_0$ (m_0 is the free electron mass). Two of these frequencies (F_α and F_β) have large oscillation amplitudes, allowing a precise assignment of oscillations to the Landau levels (LLs). Under 33 T, electrons reach the 1st LL in the α band, and the 3rd LL in the β band. By fitting the data with the Lifshitz–Onsager quantization criterion [30], we obtain the Berry phase $\sim0.67\pi$ for the 3D α band with a hole character, and $\sim0.23\pi$–0.73π for the 3D β band with an electron character at $H||c$. Further analysis of the angle dependence of the dHvA oscillations indicates that the oscillation frequencies and associated Berry phases vary significantly with respect to the direction of the applied magnetic field. Especially, the change from non-zero to zero Berry phase is observed when H is $10°$–$30°$ away from the ab plane for both α and β bands.

2. Experiment

Single crystals of PdTe$_2$ were grown via the self-flux method using excess tellurium (Te) as flux in a molar ratio of Pd:Te = 1:2.2. The starting material, Pd powder (99.95%, Alfa Aesar) and Te powder (99.99%, Alfa Aesar), was mixed together and placed into an alumina crucible, which was then sealed in a quartz tube under a vacuum of $\sim$10 millitorr. The tube was heated to 780 °C at 96 °C h^{-1} in a furnace, held at 780 °C for 48 h. The temperature was lowered to 500 °C with a rate of 3.6 °C h^{-1}. After staying at this temperature for 80 h, it was allowed to cool slowly to room temperature. Single crystals with typical size $\sim$4 $\times$ 2.5 $\times$ 0.5 mm^3 were obtained [shown in the lower panel of figure S1(a) in the supplementary material (https://stacks.iop.org/JPCM/33/035601/mmedia)].

The structure of as-grown crystals was examined through powder (crushed single crystals) x-ray diffraction (XRD)

measurements using a *PANalytical* Empyrean x-ray diffrac-
tometer (Cu K$_\alpha$ radiation; $\lambda = 1.541\,87$ Å). All the diffraction
peaks can be indexed under a CdI$_2$-type trigonal struc-
ture (space group $P\bar{3}m1$ with the lattice parameter $a = b =$
4.022 Å and $c = 5.115$ Å (see figure S1(b) in the supplemen-
tary material). The crystal symmetry and lattice parameters are
consistent with previous reports [28, 31]. Notably, each lat-
tice parameter in reference [25] is ~2.5% larger than ours. In
the absence of any explanation in reference [25], we consider
that the variation of lattice parameters is related to sample stoi-
chiometry. For example, the sample in reference [26] is slightly
Pd rich, and its lattice parameter a is closer to that in reference
[25], but c is close to ours. Through the energy dispersive spec-
troscopy (EDS), our crystals have Pd:Te ~ 0.97:2 (see figure
S1(d) in the supplementary material). The electrical resistiv-
ity was measured using the standard four-probe technique in a
physical properties measurement system (PPMS-14T, *Quan-
tum Design*). The magnetization measurements were carried
out in a superconducting quantum interference device mag-
netometer (MPMS-7T, *Quantum Design*). Magnetic torque
measurements were performed using the piezo-resistive torque
magnetometer with a 35 T resistive magnet at the National
High Magnetic Field Laboratory (NHMFL) in Tallahassee,
Florida. The dHvA oscillations were observed in both the
magnetization and magnetic torque at low temperatures ($T
\leqslant 25$ K) and high magnetic fields ($H \geqslant 1.5$ T). The
angle dependence of the magnetoresistance was also mea-
sured up to 35 T at NHMFL using the standard four-probe
technique.

3. Results and discussion

Figure 1(a) displays the temperature dependence of the electri-
cal resistivity of PdTe$_2$ along the ab plane (ρ_{ab}). Note that ρ_{ab}
decreases with decreasing temperature in the whole tempera-
ture range between 2 and 400 K with $\rho_{ab}(300$ K$) \sim 36.8\,\mu\Omega$ cm
and ρ_{ab} (2 K) $\sim 0.79\,\mu\Omega$ cm, yielding the residual resistivity
ratio (RRR) of ρ_{ab} (300 K)/ρ_{ab} (2 K) ~ 47. Such a high RRR
value and low residual resistivity reflect the high quality of our
single crystals. At high temperatures (50 K–400 K), $\rho_{ab}(T)$ is
well described by the Bloch–Gruneisen (BG) formula [32]

$$\rho(T) = \rho(0) + B_{\text{e–ph}}(T/\theta_{\text{D}})^5$$
$$\times \int_0^{T/\theta_{\text{D}}} \mathrm{d}x\, x^5 / \{[(e^x - 1)(1 - e^{(-x)})]\}, \qquad (1)$$

Here, T is the temperature, $\rho(0)$ is the residual resistivity, θ_{D}
is the Debye temperature and $B_{\text{e–ph}}$ is a constant represent-
ing the scattering strength of electrons with acoustic phonons.
From the fit, we obtain $\theta_{\text{D}} \sim 245$ K and $B_{\text{e–ph}} \sim 122\,\mu\Omega$
cm. The θ_{D} determined in this manner is slightly higher than
that obtained from specific heat measurements [33]. At low
temperatures, the experimental data gradually deviates from
the BG formula. Below 30 K, the data can be fit to $\rho_{ab}(T)
= \rho(0) + AT^m$ with $\rho(0) = 0.75\,\mu\Omega$ cm, and $m \sim 3$ (see the
inset of figure 1(a)). This indicates dominant inter-band elec-
tron–phonon scattering [34] at low temperatures (rather than
intra-band electron–phonon or electron–electron scattering),

which is consistent with a previous report [24]. Figure 1(b)
shows the temperature dependence of the magnetic suscepti-
bilities along the ab-plane (χ_{ab}) and c axis (χ_c) between 2 to
400 K measured in an applied magnetic field of 1 kOe. Over-
all, both χ_{ab} and χ_c are rather small in magnitude. While χ_{ab}
is negative and almost temperature independent in a wide tem-
perature range, χ_c is positive and increases with decreasing
temperature. The linear field dependence of the magnetization
M_{ab} (shown in figure S4(a) in the supplementary material),
indicates that the diamagnetism results from Pd and Te cores.
On the other hand, the positive χ_c should be attributed to slight
non-stoichiometry of the sample, which impacts more along
the c direction. The positive χ_c was also observed in reference
[24] but not in reference [21].

While χ_c is small, the electrical transport exhibits a large
response to the application of a magnetic field, H. Figure 1(c)
displays the transverse ($H||c$, $I||ab$) magnetoresistance
MR$_{ab} = [\rho_{ab}(H) - \rho_{ab}(0)]/\rho_{ab}(0)$ measured at a variety of
temperatures. MR$_{ab}$ is positive at all temperatures measured
and increases with decreasing temperature. For a given
temperature, MR$_{ab}$ increases with increasing field, showing
no sign of saturation. At 2 K and $H = 14$ T, it reaches 350%,
close to values previously reported [25]. For a non-magnetic
metallic system, such large and positive MR is unusual, and
cannot be simply attributed to the curving of electron
trajectories under the application of magnetic field [35, 36].

For a system with either a single band (or a dominant sin-
gle band) or multiple bands with electron–hole compensation,
the MR is expected to follow the Kohler's law [37], i.e., all
data collapses into a single curve when plotted MR$_{ab}$ versus
$H/\rho_{ab}(0)$. Figure 1(d) shows such a plot for PdTe$_2$, with all
data scaling well. The scaling curve is well described by the
form MR$_{ab} = 7.45(H/\rho_{ab}(0))^{1.3}$ as represented by the solid line
in figure 1(d). This indicates a deviation from the expected
standard Kohler form where MR $\propto H^2$. Similar behavior has
been observed in other semimetals [38, 39]. The lower power
(<2) in the field dependence is attributed to a linear-H com-
ponent that is expected when approaching the quantum limit
[24, 40]. In this sense, our MR$_{ab}$ would imply larger linear-H
component compared to that reported earlier for PdTe$_2$ where
a $H^{1.9}$ dependence was found [24]. Nevertheless, the scal-
ing behavior indicates that large MR$_{ab}$ is intrinsic and can
be described by a single electron scattering rate. If the sys-
tem contains magnetic impurities, electrons would experience
more than one type of scattering, impossible to hold the scaling
behavior.

To further understand the H dependence of the magnetore-
sistance, we measured MR$_{ab}$ with different field direction as
displayed in figure 1(e). Note that MR$_{ab}$ is always positive for
all orientation from $H \perp I$ (transverse MR$_{ab}$) to $H||I$ (longitu-
dinal MR$_{ab}$) with a progressive decrease in magnitude as the
longitudinal orientation is approached. In addition, there is an
obvious curvature change from $\theta = 0°$ to 90°, similar to what
was observed in reference [26]. This indicates the change of
the H dependence of MR$_{ab}$. In addition to the reduced con-
tribution from the Lorentz force upon the increase of θ, the
curvature changes for $\theta > 60°$ may be related to a change
in the band topology, as will be discussed later. By fitting
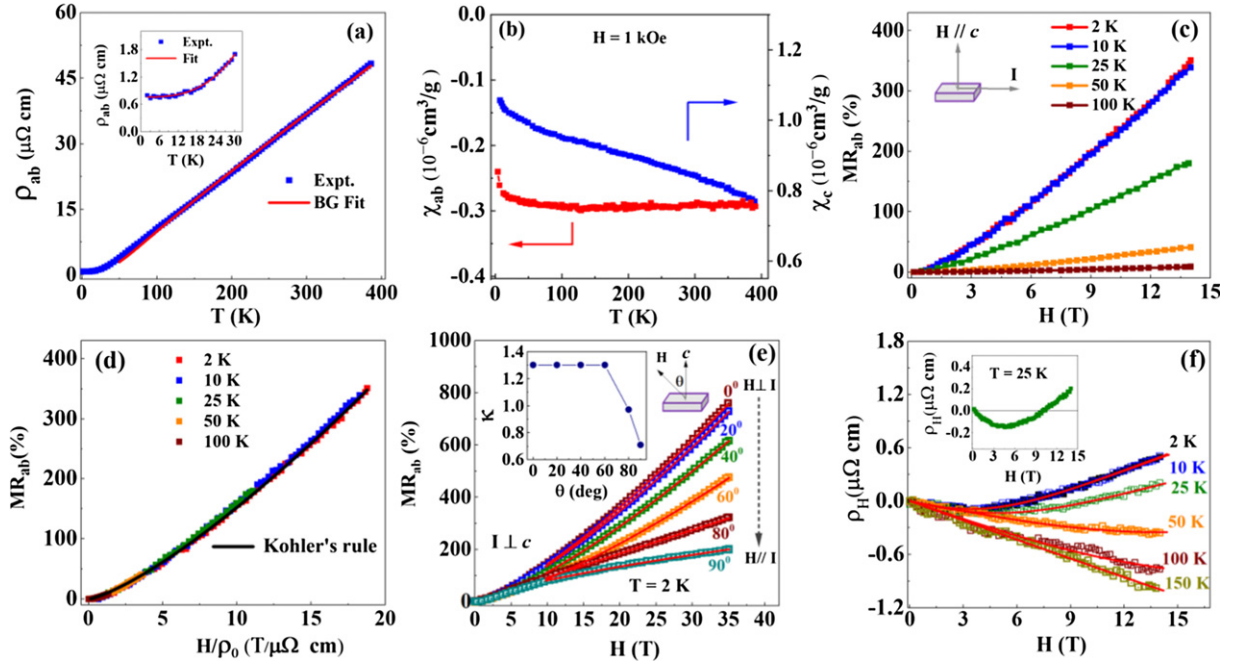
Figure 1. (a) Temperature (T) dependence of the electrical resistivity (ρ_{ab}) of PdTe$_2$. Solid line is a fit of equation (1) to the data. Upper left inset: ρ_{ab} versus T. Solid line is a fit of the form $\rho = \rho(0) + AT^m$ to the data. (b) T dependence of the magnetic susceptibility along the *ab* plane χ_{ab} (red) and the *c* axis χ_c (blue) measured by applying a magnetic field, $H = 1$ kOe. (c) Transverse magnetoresistance MR$_{ab}$ at indicated temperatures; (d) Kohler scaling plot produced using the data in frame (c). Solid line is a fit of the Kohler form to the data. (e) MR$_{ab}$ measured up to 35 T at 2 K for various angles between $H||c$ and $H||ab$ with the angle defined in the inset. Red lines represent fits of the data above 10 T to a power law MR $\propto H^\kappa$. Inset: angle dependence of the exponent κ. (f) Hall resistivity (ρ_H) measured at the temperatures indicated in the figure and the corresponding fits of equation (2) (red lines). Inset: Hall resistivity at 25 K displaying a sign change.

the high-field MR data (above 10 T) using MR$(H) \propto H^\kappa$, we determine the exponent κ for each θ, which is presented in the inset of figure 1(e). Note that there is a sharp decrease of κ at $\theta > 60°$. Nevertheless, the longitudinal MR$_{ab}$ tends to saturate at much smaller field as expected for a conventional semimetal, even though the amplitude of the magnetoresistance is still unusually high.

Figure 1(f) shows the field dependence of the Hall resistivity (ρ_H) at different temperatures. While ρ_H varies linearly with H with a negative slope at high temperatures, a nonlinearity in $\rho_H(H)$ gradually develops and becomes obvious below 50 K, leading to a sign change at low temperatures and high H (see the inset of figure 1(f)). The nonlinear Hall resistivity with a sign change clearly indicates a multiple band charge transport with contributions from both electron and hole Fermi surface pockets [21, 24, 28, 31]. Similar behavior was reported in reference [21]. To further understand the nonmonotonic field dependence of the Hall resistivity, we use the two-band model [41, 42] to describe our experimental data,

$$\rho_{xy}(H) = \frac{H}{e} \frac{(n_h\mu_h^2 - n_e\mu_e^2) + (n_h - n_e)\mu_h^2\mu_e^2 H^2}{(n_h\mu_h + n_e\mu_e)^2 + (n_h - n_e)^2\mu_h^2\mu_e^2 H^2} \quad (2)$$

where $n_h(n_e)$ is the concentration of holes (electrons) and $\mu_h(\mu_e)$ is the mobility of holes (electrons). The fitting results are displayed in figure S2 (supplementary material). While they show weak temperature dependence at high temperatures (>50 K), both n_h and n_e decrease with decreasing temperature. At 2 K, $n_h \sim 1.6 \times 10^{22}$ cm^{-3} and $n_e \sim 0.62 \times 10^{22}$ cm^{-3},

while $\mu_h \sim 0.11 \times 10^4$ cm^3 V^{-1} s^{-1} and $\mu_e \sim 0.59 \times 10^4$ cm^3 V^{-1} s^{-1}. These mobilities are close to that of PtTe$_2$ [24] and PtBi$_2$ [39]. The carrier concentrations are close to that obtained from the thermopower measurement [43]. We also note that the ratio $n_h/n_e \neq 1$, implying uncompensated electrons and holes in PdTe$_2$.

Figure 2(a) displays the H dependence of the magnetization, $M(H)$, measured along the *c* axis ($H||c$) at 1.8 K. Note that there are pronounced dHvA oscillations above 1.5 T. The emergence of the dHvA oscillations is the consequence of the Landau level formation in the presence of magnetic field [30, 44]. When the magnetic field varies, the quantized Landau levels pass over the Fermi surface, resulting in the oscillation of the electronic density of states at the Fermi level. This leads to the oscillations of physical quantities including the magnetization and magnetic torque [13]. In the low field regime, a non-linear behavior can be seen for each temperature measured (see the inset of figure 2(a)). As discussed above, the non-linear $M(H)$ is likely associated with the slight non-stoichiometry of the sample. However, whether the background is positive (reference [24]) or negative (reference [21]) does not seem to impact the dHvA oscillations, judged from observed frequencies (see table 1). The non-oscillatory part (smooth background) of the magnetization data is obtained by fitting the low-field magnetization using polynomial formula (the orange curve), which is subtracted from the data to obtain the oscillatory part of the magnetization ΔM, as plotted in figure 2(b). From the fast Fourier transformation (FFT)
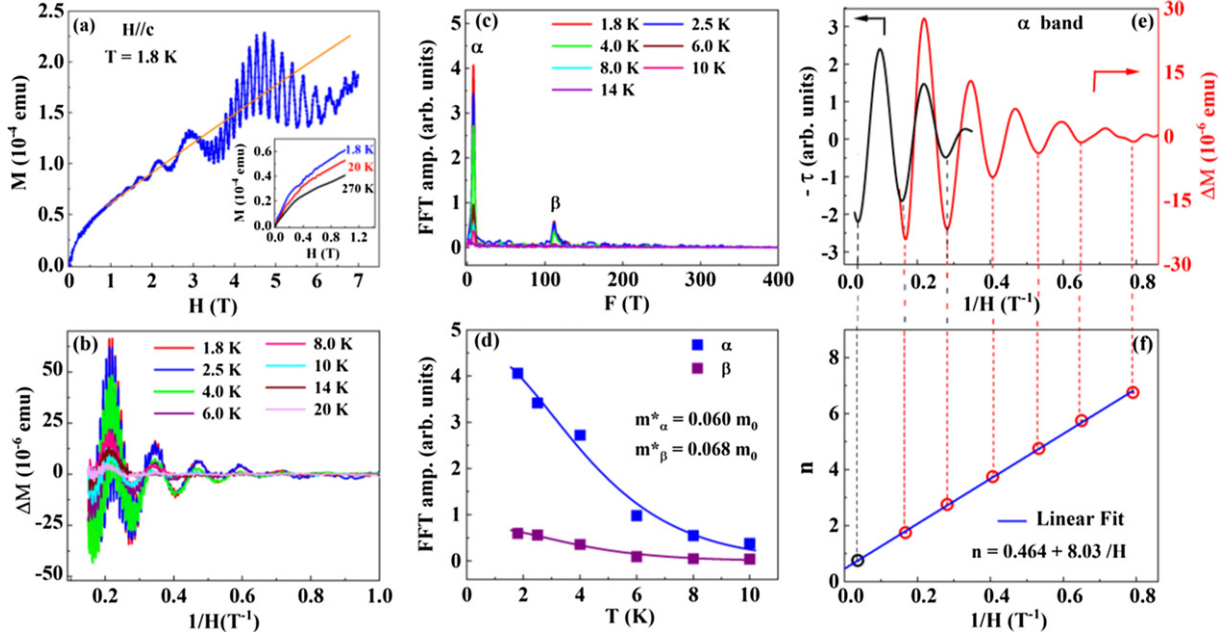
Figure 2. (a) Magnetization (M), vs magnetic field (H) of PdTe$_2$ at 1.8 K; Inset: low-field $M(H)$ at the indicated temperatures. Orange line represents the non-oscillatory part (smooth background) of the magnetization. (b) dHvA oscillations after the subtraction of the non-oscillatory part of M (ΔM) at the indicated temperatures; (c) FFT of ΔM at the indicated temperatures. (d) Temperature dependence of the FFT amplitude observed in frame (c) for the α and β bands. Solid lines are fits with thermal damping term of equation (3); (e) dHvA oscillation of ΔM (red) and τ (black) at 1.8 K. (f) Landau fan diagram constructed from the dHvA oscillation corresponding to the α band in ΔM in frame (e).

of the data shown in figure 2(c), two oscillations are identified with the frequencies $F_\alpha = 8$ T and $F_\beta = 117$ T.

According to the Lifshitz–Kosevich formula [29, 44],

$$\Delta M \propto - H^{1/2} \frac{A(\frac{m^*}{m_0})T}{\sinh(A(\frac{m^*}{m_0})T)} \ \exp\left\{-A\left(\frac{m^*}{m_0}\right)T_D\right\}$$
$$\times \ \cos(\pi g m^*/2m_0) \sin\left[2\pi\left\{\frac{F}{H} - \left(\frac{1}{2} - \Phi\right)\right\}\right],$$
$$(3)$$

where $\frac{A(\frac{m^*}{m_0})T}{\sinh(A(\frac{m^*}{m_0})T)}$ is the thermal damping factor, $\exp\{-A(\frac{m^*}{m_0})T_D\}$ is the Dingle damping factor, T_D is the Dingle temperature, $\cos(\pi g m^*/2m_0)$ is the spin reduction factor, $A = \frac{2\pi^2 k_B m_0}{e\hbar H}$, m^* is the effective mass of electron, and g is the Landé factor. In addition, $\Phi = \frac{\Phi_B}{2\pi} + \delta$ where Φ_B is the Berry phase and $\delta = 0$ for a two-dimensional (2D) and $+/-$ 1/8 for a three-dimensional (3D) Fermi surface (FS). Here $+/-$ sign corresponds to the minima $(+)$/maxima $(-)$ of the cross-sectional area of the FS for the case of an electron band. For a 3D hole band, the sign of δ is opposite [45]. The phase analysis of these dHvA oscillations makes it possible to reveal the topological properties of the associated carriers through the determination of Φ_B. A non-zero value of Φ_B corresponding to the dHvA oscillation is an indication of the presence of non-trivial topology [44].

Figure 2(d) exhibits the temperature dependence of the FFT amplitudes for both the α and β bands. From a fit of the thermal damping factor $\frac{A(\frac{m^*}{m_0})T}{\sinh(A(\frac{m^*}{m_0})T)}$ to the temperature dependence of the FFT amplitude, we obtain $m^*_\alpha = 0.060 m_0$ and $m^*_\beta = 0.068 m_0$. Both of these values are smaller than that reported previously [21] but somewhat larger than that reported in reference [24].

According to the Onsager relation, $F = (\Phi_0/2\pi^2)S$, where Φ_0 is the flux quanta and S is the cross-section area of the Fermi surface normal to the H direction. For the α band, we found $S_\alpha \sim 0.076$ nm^{-2}, which corresponds to the Fermi wave vector $k_\alpha \sim 0.015$ Å^{-1}. This wave vector is close to that of expected from DFT calculations for a small hole pocket around the Γ point [21, 24] of the Brillouin zone (BZ). We notice that the dHvA oscillation due to the α band was not detected in reference [25], suggesting that the Fermi level is sample sensitive as suggested in reference [24]. For the β band, we find $S_\beta \sim 1.115$ nm^{-2} and the corresponding Fermi wave vector $k_\beta \sim 0.059$ Å^{-1}. This value is close to that corresponding to the electron pocket located between A to H points in the BZ as reported in the published DFT calculations [15, 21].

To assign Landau levels for each oscillation, we separate ΔM for each frequency via the filtering process [24, 45]. Figure 2(e) shows ΔM versus $1/H$ (red curve) for the α band isolated by using a low-pass filter of 20 T. The Landau fan diagram can be constructed by assigning the oscillation minima
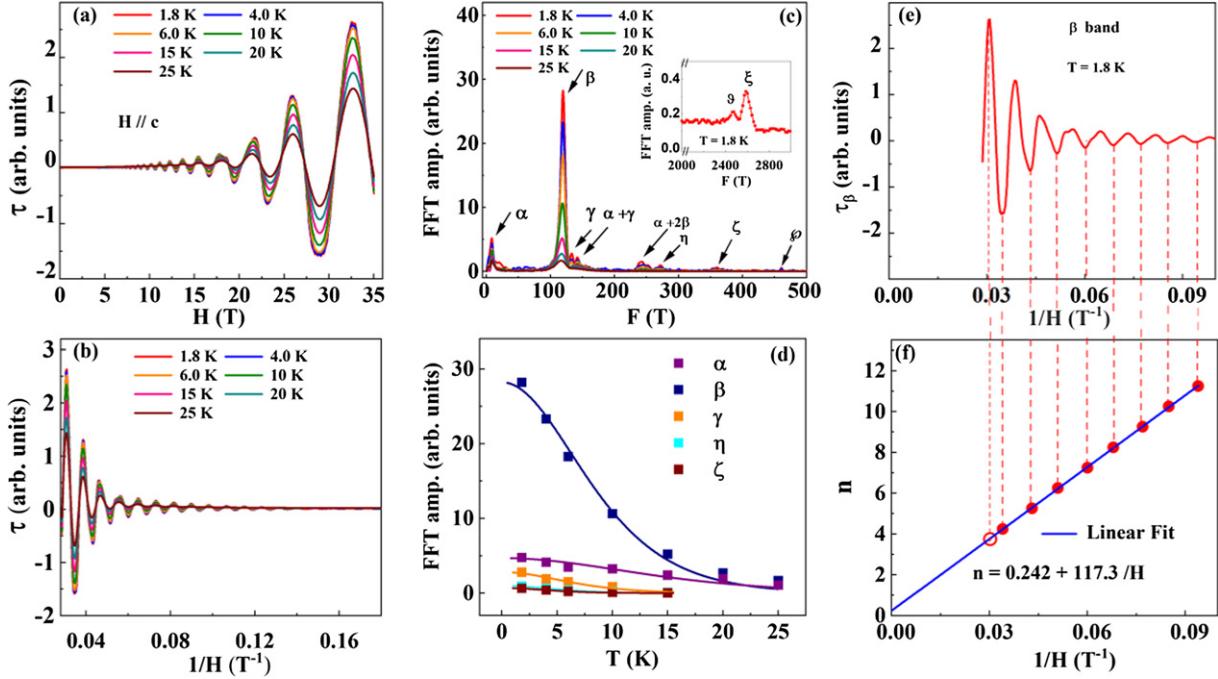
Figure 3. (a) Field dependence of the magnetic torque (τ) of PdTe$_2$ at the indicated temperatures; (b) τ versus $1/H$. (c) FFT of τ at the indicated temperatures, Inset: FFT of τ at 1.8 K displaying high frequencies. (d) Variation of FFT amplitude with temperature for respective bands as indicated. The solid lines are fits with thermal damping term of equation (3). (e) dHvA oscillation at 1.8 K from the β band. (f) Landau fan diagram constructed from the data presented in frame (e).

to $n - 1/4$ with n being the Landau level index [44]. As shown in figure 2(f), $n(H^{-1})$ can be fitted with the Lifshitz–Onsager quantization criterion [30] as $n = 0.46 + 8.03/H$. From the fit, we obtain the frequency $F_\alpha = 8.03$ T, in excellent agreement with that obtained from the FFT spectra. This implies that the filtering process to isolate the α band preserves the original signal. The intercept of this linear equation gives the Berry phase as $(\Phi_B^\alpha/2\pi) + \delta = 0.46$, i.e.$\Phi_B^\alpha = 0.92\pi - 2\pi\delta$. Similar intercept value was also reported in references [21, 24]. However, the corresponding Berry phase is considered to be nontrivial in reference [21] but trivial in reference [24] due to different interpretations of calculated electronic structures. In either case, the dimensionality factor (δ) has been completely ignored [21, 24, 26, 27]. According to reference [21], the α band corresponds to a hole pocket and nearly isotropic (to be discussed later), $\delta = 1/8$ is expected corresponding to the maximum cross-section [46] for $H||c$. We thus obtain the Berry phase $\Phi_B^\alpha = 0.67\pi$, indicating a topologically nontrivial phase. The nontrivial topology of the α band is consistent with the theoretical calculations (tilted Dirac cone along the Γ–A direction hosting type-II Dirac fermions) and ARPES measurements [17, 21].
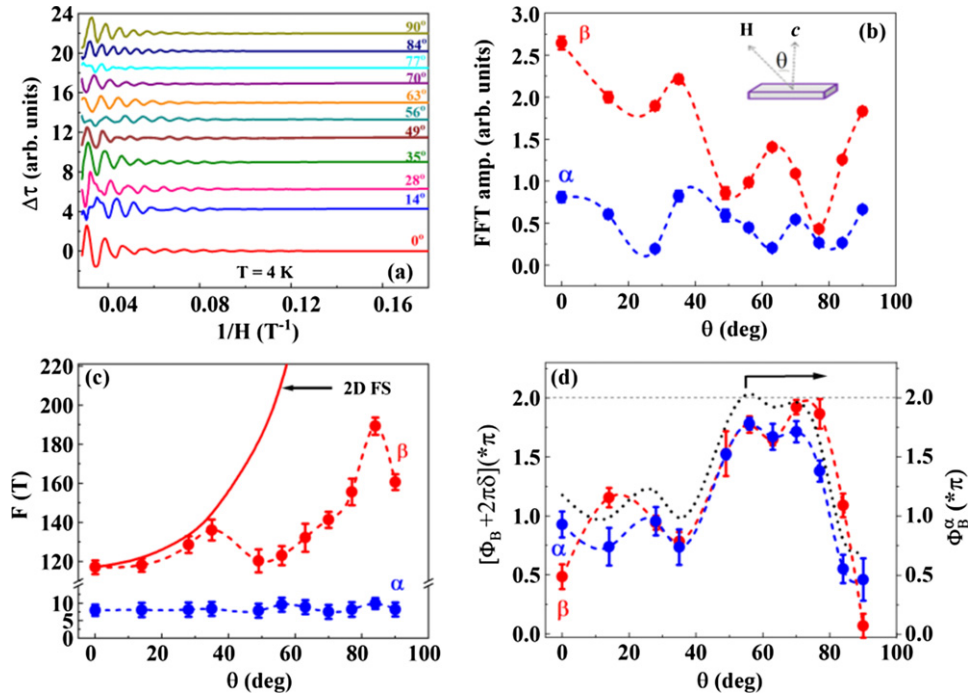
Under 7 T, the carriers in the α band can reach the 2nd Landau level (LL), while the carriers in the β band are far from the quantum limit. The intercept obtained from the linear extrapolation from such high LLs will have a large uncertainty. To better determine the high field intercept and hence the precise Berry phase, we have carried out magnetic torque measurements of PdTe$_2$ for fields up to 35 T. Figure 3(a) shows the field dependence of the magnetic torque measured under $H||c$ at several temperatures. As expected, the dHvA oscillations

become more pronounced upon an increase of H. The dHvA oscillations plotted against the inverse magnetic field (H^{-1}) are shown in figure 3(b). Through the FFT analysis as shown in figure 3(c), we can identify eight frequencies, which are α (8 T), β (117 T), γ (133 T), η (272 T), ζ (360 T), $\wp$ (462 T), ϑ (2468 T), and ξ (2588 T). While six of these frequencies (8 T, 117 T, 133 T, 462 T, 2468 T, and 2588 T) have been reported previously [21, 24], both η (272 T) and ζ (360 T) are new findings. Two additional peaks in figure 3(c) correspond to the sum of α and γ of 141 T and the sum of α and 2β of 242 T. Two high frequencies (2468 T and 2588 T) we observed were reported in reference [24] but not in references [21, 25]. As summarized in table 1, literature shows discrepancies in the frequencies, which may be related to the subtle difference between samples or the method employed to measure them. This suggests that the Fermi surface pockets in PdTe$_2$ have not been well characterized [28].

Figure 3(d) displays the temperature dependence of the FFT amplitude for each of the indicated frequencies. The FFT amplitude decreases with increasing temperature for all frequencies as expected. Fitting our data using the thermal damping term of equation (3), we obtain the effective mass of the carriers for each band. These results are summarized in table 2 along with S_F and k_F. Note that m_α^* and m_β^* extracted from the magnetic torque are almost identical to those obtained from $M(H)$. The high m_η^* compared to m_γ^* suggests that F_η is not the 2nd harmonic oscillation of the γ band. To investigate the dynamics of the carriers, we estimate T_D through the Dingle plots (shown in figure S3, supplementary material).

Table 2. Parameters obtained from the dHvA oscillations in PdTe$_2$ at $H||c$ including the oscillation frequency (F), the Fermi wave vector (k_F), the effective mass (m^*), the Fermi velocity (v_F), the Dingle temperature T_D, the quantum relaxation time (τ_q), the quantum mobility (μ_q) and the mean free path (λ).

Band	F (T)	S_F (10^{-2} Å^{-2})	k_F (Å^{-1})	m^*/m_0	v_F (10^5 m s^{-1})	T_D (K)	τ_q (10^{-13} s)	μ_q (m^2 V^{-1} s^{-1})	λ (nm)
α	8.0	0.076	0.015	0.059	2.9	2.30	5.0	1.465	145
β	117	1.115	0.059	0.067	10.1	32.0	0.37	0.097	37.4
γ	133	1.268	0.063	0.084	8.7	—	—	—	—
η	272	2.593	0.090	0.107	9.7	—	—	—	—
ζ	360	3.432	0.104	0.120	9.9	—	—	—	—
$\wp$	462	4.405	0.118	—	—	—	—	—	—
ϑ	2468	23.53	0.273	—	—	—	—	—	—
ξ	2588	24.67	0.280	—	—	—	—	—	—

Figure 4. (a) Magnetic torque of PdTe$_2$ at 4 K after background subtraction plotted as $\Delta\tau(H)$ versus H^{-1} for different angles as indicated. A constant offset is added to the data for display purpose. (b) Angle dependence of the FFT amplitude for the α and β bands. (c) Angle dependence of F_α and F_β. The error bars are taken as the half-width at the half-height of the FFT peaks. Solid line represents the angular dependence expected for a 2D Fermi surface. (d) Angle dependence of $\Phi_B + 2\pi\delta$ for the α and β bands. Dotted line depicts the angle dependence of Φ_B for the α band assuming $\delta = 1/8$. Dashed lines in (b)–(d) panels are guides to the eye.

From T_D, m^* and k_F, we calculate the quantum relaxation time $\tau_q = \frac{\hbar}{2\pi T_D k_B}$, quantum mobility $\mu_q = \frac{e\tau_q}{m^*}$, Fermi velocity v_F, and mean free path $\lambda = v_F \tau_q$, which are listed in table 2. For the α band, the long τ_q and small m^* lead to an extremely high quantum mobility, which is almost two times higher than that reported previously [21], reflecting high quality of our single crystal samples. Compared to the α band, the β band has much smaller τ_q and λ, even though its velocity is higher.

Since $\vec{\tau} = \vec{M} \times \vec{H}$, the dHvA oscillations in the magnetic torque can be in phase or out of phase with that in the magnetization ($\tau = -\frac{1}{F}\frac{dF}{d\theta}M_{//}H$, where $M_{||}$ is the component of M parallel to H [44]). As shown in figure 2(e), τ (black) is out of phase with ΔM. Nevertheless, dHvA oscillations obtained from τ overlaps well with that from ΔM. Under 35 T, carriers in the α band reaches the 1st LL (figure 2(e)). By indexing

the LLs from the dHvA oscillations corresponding to the β band shown in figure 3(e), we find that high field (35 T) can push the carriers down to the 3rd LL. The oscillation due to the β band is isolated via a band-pass filter centered about F_β, so to avoid possible contributions of other nearby frequencies. Although $F_\beta = 117$ T has been reported [21, 24, 25], its Berry phase remains unknown. Figure 3(f) shows the Landau fan diagram for the β band. From the intercept of the linear fit, we obtain $\Phi_B^\beta/2\pi = 0.242 - \delta$. As the β band is an electron pocket [21, 24], we find the Berry phase $\Phi_B^\beta = 0.23\pi$ (with $\delta = +1/8$ for a FS minimum) $- 0.73\pi$ (with $\delta = -1/8$ for a maximum FS). While a non-zero Φ_B^β implies a nontrivial Berry phase, the β band is not predicted to be involved in a nontrivial band crossing according to the DFT calculations in reference [21].

The angular dependence of quantum oscillations can provide further information about the Fermi surface topology. Figure 4(a) shows the magnetic torque at $T = 4$ K after background subtraction plotted as $\Delta\tau(H)$ versus H^{-1} for different angles θ as defined in the inset of figure 4(b). Upon the variation of θ, the dHvA oscillations change in both amplitude and peak position. Through the FFT analysis (see figure S5, supplementary material), we can track the dominant α and β bands for all measured angles. However, the amplitudes associated with higher frequencies (γ, η, ζ, $\wp$, ϑ and ξ) gradually vanish at $\theta > 28°$. To precisely analyze the amplitude variation with θ for the α and β bands, we separate their contributions through the band-pass filtering (shown in figures S6 and S7, supplementary material). Figure 4(b) displays the angle dependence of the FFT amplitude for the α and β bands. The amplitude varies non-monotonically with θ for the both bands. Such non-monotonic variation of the FFT amplitude is attributed to the spin reduction factor $\cos(\pi g m^*/2m_0)$ (see equation (3)). Our measurement of the dHvA oscillations under $H||ab$ (see figure S4(d), supplementary material) allows to determine $m_\alpha^* = 0.079m_0$ and $m_\beta^* = 0.092m_0$. These values of the effective masses are close to that found for $H||c$. We therefore consider that the change in m^* does not significantly alter $\cos(\pi g m^*/2m_0)$ and that the amplitude variation of the dHvA oscillations is due to the variation of g, which is related to spin–orbit coupling. When changing the magnetic field direction, a modification on the g factor is expected [47]. When $g\frac{m^*}{m_0} = 2l + 1$ (l is an integer), the oscillation vanishes, a phenomenon known as the spin zero effect [44, 48]. Such an effect has been suggested for the band with 109 T frequency of PdTe$_2$ [24]. In contrast, our FFT amplitude data for both the α and β bands tends to vary greatly and is significantly reduced around 77° but does not completely vanish suggesting that the spin zero effect is not satisfied by these bands.

Figure 4(c) displays the angle dependence of F_α and F_β. F_β exhibits a non-monotonic angle dependence, while F_α is only weakly angle dependent. Apparently, neither the α nor β band possesses 2D Fermi surface character as represented by the solid curve in figure 4(c). While the angular dependence of F_α and F_β has been previously reported up to $\theta \sim 60°$ [24], our data provides information in the range of $0° \leqslant \theta \leqslant 90°$. By constructing the Landau fan diagram from the dHvA oscillations at each angle measured (shown in figures S6 and S7, supplementary material), the corresponding phase $\Phi_B + 2\pi\delta$ is extracted. Figure 4(d) displays $\Phi_B + 2\pi\delta$ versus angle for both α and β bands, both displaying a non-monotonic variation from $H||c$ towards $H||ab$. Despite the small anisotropy of the α frequency, $\Phi_B + 2\pi\delta$ strongly depends on the orientation of the applied field. If we assume $\delta = 1/8$ for all field direction, $\Phi_B \sim 2\pi$ for the α band at $50°$–$75°$. As discussed earlier, there is a sharp change in the curvature of MR (see figure 1(e)) around 77°. Interestingly, the quantity $\Phi_B + 2\pi\delta$ for the β frequency also reaches 2π (i.e., zero) at 77° at which the oscillation amplitudes reach minimum. Understanding of the variation of the Berry phase with angle that we observe here requires further theoretical investigation.

4. Summary

In summary, we have measured the charge transport properties (resistivity, magnetoresistance, and Hall resistivity), as well as the magnetic (magnetization and magnetic torque) properties of PdTe$_2$ single crystals with RRR ~ 47. While our magnetoresistance data exhibits Kohler-type scaling behavior, the MR displays an unusual $H^{1.3}$ dependence, suggesting contributions from multiple bands, as reflected in the Hall resistivity (with nonlinear-H dependence and sign change). Pronounced dHvA oscillations are observed in the magnetization and magnetic torque at low temperatures. Through the analysis of the observed dHvA oscillations, eight bands are identified with frequencies: 8 T, 117 T, 133 T, 272 T, 360 T, 462 T, 2468 T, and 2588 T for $H||c$, the two intermediate frequencies (i.e. 272 T and 360 T) have not been previously reported, to our knowledge. Among these, the α band (8 T when $H||c$) and β (117 T when $H||c$) are the most dominant contributions. The angle dependence of F_α and F_β indicates a 3D character of the corresponding bands. For the first time, the angle dependence of the Berry phase of the α and β bands of PdTe$_2$ are obtained, displaying a variation from nontrivial to trivial at an angle of 77° between H and the crystallographic c axis for the α and β bands. At present, it is not clear whether both the α and β bands are associated with a type-II Dirac cone which has been predicted to lie about 0.5 eV below the Fermi energy [21, 24].

Acknowledgments

ORCID iDs

Ramakanta Chapai ⬤ https://orcid.org/0000-0002-9227-4492
Rongying Jin ⬤ https://orcid.org/0000-0001-5846-4324

References

[1] Borisenko S, Gibson Q, Evtushinsky D, Zabolotnyy V, Buchner B and Cava R J 2014 *Phys. Rev. Lett.* **113** 027603
[2] Neupane M *et al* 2014 *Nat. Commun.* **5** 3786
[3] Xu S-Y *et al* 2015 *Science* **347** 294
[4] Weng H, Fang C, Fang Z, Bernevig B A and Dai X 2015 *Phys. Rev.* X **5** 011029
[5] Huang S, Kim J, Shelton W A, Plummer E W and Jin R 2017 *Proc. Natl Acad. Sci. USA* **114** 6256
[6] Banerjee A *et al* 2016 *Nat. Mater.* **15** 733
[7] Bhattacharjee Q L, Pan L, Stern A L, Burks E C, Che X, Yin G, Wang J, Lian B, Zhou Q, Choi E S *et al* 2017 *Science* **357** 294

[8] Bradlyn B, Cano J, Wang Z, Vergniory M G, Felser C, Cava R J and Bernevig B A 2016 *Science* **353** 5037
[9] Chapai R, Jia Y, Shelton W A, Nepal R, Saghayezhian M, DiTusa J F, Plummer E W, Jin C and Jin R 2019 *Phys. Rev. B* **99** 161110(R)
[10] Chen Y L *et al* 2009 *Science* **325** 178
[11] Hasan M Z and Kane C L 2010 *Rev. Mod. Phys.* **82** 3045
[12] Hor Y S *et al* 2010 *Phys. Rev. Lett.* **104** 057001
[13] Ando Y J 2013 *J. Phys. Soc. Japan* **82** 102001
[14] Sato M and Ando Y 2017 *Rep. Prog. Phys.* **80** 076501
[15] Bahramy M S *et al* 2018 *Nat. Mater.* **17** 21
[16] Cooil M *et al* 2017 *Nat. Commun.* **8** 257
[17] Noh H J, Jeong J, Cho E J, Kim K, Min B I and Park B G 2017 *Phys. Rev. Lett.* **119** 016401
[18] Leng H, Paulsen C, Huang Y K and de Visser A 2017 *Phys. Rev. B* **96** 220506(R)
[19] Yan B and Felser C 2017 *Annu. Rev. Condens. Matter Phys.* **8** 337
[20] Armitage N P, Mele E J and Vishwanath A 2018 *Rev. Mod. Phys.* **90** 015001
[21] Fei F *et al* 2017 *Phys. Rev. B* **96** 041201(R)
[22] Liu Y *et al* 2015 *Chin. Phys. Lett.* **32** 067303
[23] Okamoto H 1992 J Phase Equilibria **13** 73
[24] Zheng W *et al* 2018 *Phys. Rev. B* **97** 235154
[25] Wang Y *et al* 2016 *Sci. Rep.* **6** 31554
[26] Amit S R K, Singh A, Wadehra N, Chakraverty S and Singh Y 2018 *Phys. Rev. Mater.* **2** 114202
[27] Das S, Amit S A, Yadav L, Gayen S, Singh Y and Sheet G 2018 *Phys. Rev. B* **97** 014523
[28] Dunsworth A E 1975 *J. Low Temp. Phys.* **19** 51
[29] Lifshitz I E and Kosevich A M 1956 *Sov. Phys - JETP* **2** 636
[30] Ashcroft N W and Mermin N D 1976 *Solid State Physics* (New York: Holt, Rinehart and Winston)
[31] Jan J-P and Skriver H L 1977 *J. Phys. F: Met. Phys.* **7** 1719
[32] Blatt F J 1968 *Physics of Electronic Conduction in Solids* (New York: McGraw-Hill)
[33] Kudo K, Ishii H and Nohara M 2016 *Phys. Rev. B* **93** 140505(R)
[34] Ziman J M 2001 *Electrons and Phonons: The Theory of Transport Phenomena in Solids* (Oxford: Oxford University Press)
[35] Abrikosov A A 1988 *Fundamentals of the Theory of Metals* (Amsterdam: North-Holland)
[36] Pippard A B 1989 *Magnetoresistance in Metals* (Cambridge: Cambridge University Press)
[37] Duan F and Guojun J 2005 *Introduction to Condensed Matter Physics* vol 1 (Singapore: World Scientific)
[38] Wang Y L *et al* 2015 *Phys. Rev. B* **92** 180402(R)
[39] Xing L, Chapai R, Nepal R and Jin R 2020 *npj Quantum Mater.* **5** 10
[40] Wang K, Graf D and Petrovic C 2013 *Phys. Rev. B* **87** 235101
[41] Gao W *et al* 2017 *Phys. Rev. Lett.* **118** 256601
[42] Luo Y *et al* 2015 *Appl. Phys. Lett.* **107** 182411
[43] Hooda M K and Yadav C S 2018 *Europhys. Lett.* **121** 17001
[44] Shoenberg D 2009 *Magnetic Oscillations in Metals* (Cambridge: Cambridge University Press)
[45] Xia W *et al* 2020 *Appl. Phys. Lett.* **116** 142103
[46] Li C, Wang C M, Wan B, Wan X, Lu H Z and Xie X C 2018 *Phys. Rev. Lett.* **120** 146602
[47] Gharaati A 2017 *Solid State Commun.* **258** 17
[48] Bi R, Feng Z, Li X, Niu J, Wang J, Shi Y, Yu D and Wu X 2018 *New J. Phys.* **20** 063026